ISSN (Print) 1226-1750
ISSN (Online) 2233-6656
Journal of Magnetics 22(3), 378-381 (2017) https://doi.org/10.4283/JMAG.2017.22.3.378

Birdcage Coil with Inductively Coupled RF Coil Array for Improving $|B_1|$-Field Sensitivity In 7-T MRI

Jong-Deok Byun[1], Jeung-Hoon Seo[2], Taewon Kang[1], Yeunchul Ryu[3], and Kyoung-Nam Kim[4]*

[1]*Department of Mechanical and Biomedical Engineering, Kangwon National University, Kangwon-do 24341, Korea*
[2]*Neuroscience Research Institute, Gachon University, Incheon 21565, Korea*
[3]*Department of Radiological Science, Gachon University, Incheon 13120, Korea*
[4]*Department of Biomedical Engineering, Gachon University, Incheon 13120, Korea*

(Received 2 May 2017, Received in final form 2 August 2017, Accepted 2 August 2017)

A birdcage coil integrated with a 16-channel, inductively coupled, radio-frequency (RF) array was designed to improve the magnetic-flux distribution for human brain magnetic resonance imaging at 7-T. A numerical calculation was performed using the finite-difference time-domain method for the birdcage coil with an inductively coupled array. The electromagnetic calculation results for the birdcage coil with the inductively coupled array were compared to those for the birdcage coil without an inductively coupled array in terms of their magnetic-flux, electric-field, and specific-absorption-rate distributions in a cylindrical phantom and human model. The proposed birdcage coil with an inductively coupled array offers a superior magnetic-flux sensitivity without sacrificing the RF power deposition at 7-T. The modifications of the coil geometry accompanying the inductively coupled RF array could be applied to the generally used transmit/receive volume coils and extended to parallel RF transmission array in ultra-high-field magnetic resonance imaging.

Keywords : Magnetic Resonance Imaging (MRI), Radio-Frequency (RF) coil, Inductively Coupled Coil, 7-Tesla (T)

1. Introduction

The magnetic resonance imaging (MRI) quality characteristics such as the signal-to-noise ratio and contrast-to-noise ratio are strongly affected by the performance of the radio-frequency (RF) coil [1, 2]. In particular, in ultra-high field (UHF, $\geq$ 7-T) MRI, the homogeneous magnetic-flux ($|B_1|$) distribution and its sensitivity present challenges because of the limitations imposed by the shortened RF wavelength in biological tissues characterized by high dielectric constants, namely, permittivity and conductivity [3]. In response to these needs, the design and engineering of RF coils have increasingly integrated sustainability into new approaches such as the attachment of a high permittivity material to the coil, modified coil geometries, and a hybrid configuration that includes a supplementary coil in addition to the existing coil.

For volumetric MRI such as brain, body, or knee imaging, the birdcage (BC) geometry is being increasingly incorporated in MRI instruments due to the high sensitivity of the $|B_1|$-field and its uniform distribution [4, 5]; thus, for research or clinical purposes, geometries or modified geometries of BC coils such as a spiral shape and an additional end-cap configuration have been suggested. In clinical approaches, the BC coil is utilized in the local transmit (Tx)-only or transmit/receive (Tx/Rx) modes. By contrast, various BC coil geometries have been used for specific-target imaging. Generally, the BC coil comprises two circular conductive loops corresponding to the end ring (ER) and a straight conductor that is referred to as a leg or rung [6]. The large number of straight conductors is the direct cause of and is proportional to the high $|B_1|$-field sensitivity and homogeneity [7]. However, the use of a large number of straight conductors is restricted in practical MR applications owing to the mutual interference between the legs.

Herein, a BC coil with an inductively coupled (IC) array (*w*-IC BC) is proposed to improve its $|B_1|$-field sensitivity for 7-T brain imaging, and its performance is compared to a BC coil without the IC coil array (*wo*-IC BC) in terms of their $|B_1|$-field, electric ($|E|$)-field, and specific-absorption-rate (SAR) distributions in a cylin-

*Corresponding author: Tel: +82-32-460-9060
Fax: +82-32-460-8230, e-mail: kyoungnam.kim@gachon.ac.kr

drical phantom and computational biological human-head model.

2. Materials and Methods

To evaluate the performance of the *w*-IC BC configuration, electromagnetic (EM)-field calculations were performed using the XFDTD software (Remcom, Inc., State College, PA, USA), and the results were compared to the results obtained for the standard coil configuration of the *wo*-IC BC. The voxel size for the field calculation was set to 372 × 372 × 190 Yee cells for the oil-based homogeneous phantom and to 522 × 372 × 340 Yee cells for the computational biological human-head model, each with the 1-mm resolution in the x, y, and z directions.

The 48 sinusoidal RF sources for RF excitation in the band-pass filter (BPF) BC coil were assigned as 16 sources at the intermediate locations of the straight conductors and 32 sources at the ERs. The two coil configurations were compared using the results obtained for a cylindrical phantom (Figs. 1(a) and (b)) and human-head model (Figs. 1(c) and (d)). The coil geometry can be classified into two types, namely, the *wo*-IC BC (Figs. 1(a) and (c)) and *w*-IC BC (Figs. 1(b) and (d)). The diameter and length of the model BC coil were 330 and 150 mm, respectively. The 16-channel IC coil array was modeled with the diameter of 280 mm and the length of 150 mm, and the width and length of a single element were 40 and 150 mm, respectively. The IC coil array was positioned at the isocenter of the external BC coil.

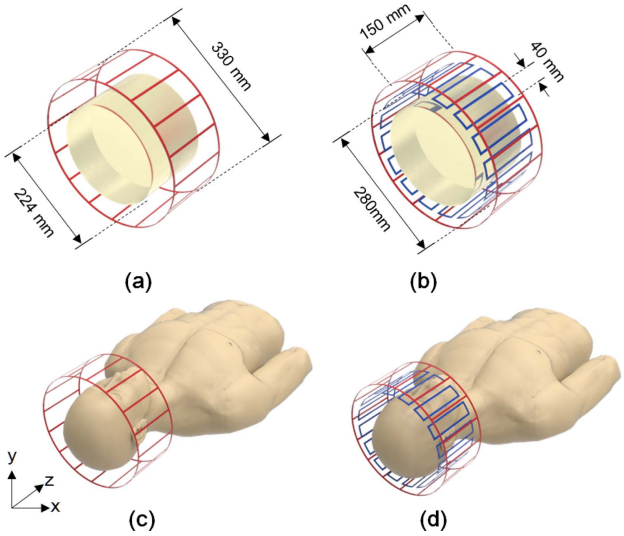

Fig. 1. (Color online) Geometric models of the *wo*-IC BC and *w*-IC BC for the finite-different time-domain calculation: (a) *wo*-IC BC (only BC) using the oil-based phantom, (b) *w*-IC BC (BC + IC array) using the oil-based phantom, (c) *wo*-IC BC (only BC) using the human phantom, and (d) *w*-IC BC (BC + IC array) using the human phantom.

Two coil geometries were modeled using AutoCAD 2015 (Autodesk Inc., San Rafael, CA) given by the SAT file. Each leg of the BC and IC coil array was divided into four sectors with the clearance of 37.5 mm. In the BC coil, a current source was utilized for RF excitation and reception. However, a 6.26-pF tuning capacitor (C_T) was used in the IC coil array. In the phantom model, an oil-based homogeneous phantom was designed with the diameter and length of 224 and 150 mm, respectively. The conductivity and relative permittivity were 0 $S \cdot m^{-1}$ and 4, respectively [8]. The computational human-head model (Visible Human Data; contains 17 materials) was taken from XFDTD. In the computational analysis, the RF excitation ($|B_1^+|$) field was calculated according to the reciprocity principle [9]. The central pixel in the acquired $|B_1^+|$-field of the BC coil was calculated when the flip angle during MR acquisition was assumed to be 90° and normalized at 1.95 μT. To evaluate the $|B_1^+|$-field uniformity, homogeneity factor (HF) values were compared *w*-IC BC and *wo*-IC BC, with HF defined as follows [10]:

$$HF[\%] = 100 \times \left[1 - \frac{(MAX_{Signal} - MIN_{Signal})}{(MAX_{Signal} + MIN_{Signal})}\right],$$

where MAX_{Signal} and MIN_{Signal} are the maximum and minimum $|B_1^+|$ signals, respectively.

3. Results and Discussion

The $|B_1|$-, $|B_1^+|$-, and $|B_1^-|$-field distributions in the *wo*-IC BC (Figs. 2(a) and (c)) and *w*-IC BC (Figs. 2(b) and (d)) obtained computationally using the oil-based cylindrical phantom were compared. The intensities of the $|B_1|$-fields at the central region were measured to be 3.40 × 10^{-6} and 4.01 × 10^{-6} μT for the *wo*-IC BC and *w*-IC BC, respectively (Figs. 2(a) and (b)). These results indicate that the sensitivity of the $|B_1|$-field map of the *w*-IC BC is 15% higher than that of the *wo*-IC BC. The $|B_1|$-field can be categorized into two field components, the $|B_1^+|$- and $|B_1^-|$-fields, representing the RF excitation and RF reception sensitivity, respectively [11]. The HF values given by the $|B_1^+|$-field maps were measured to be 96.83 and 97.11 for the *wo*-IC BC and *w*-IC BC, respectively. In the $|B_1^-|$-field maps, the $|B_1^-|$-field sensitivities were calculated to be 4.94 × 10^{-7} and 5.74 × 10^{-7} μT for the *wo*-IC BC and *w*-IC BC, respectively.

For the biological human-head model, the $|B_1|$-, $|B_1^+|$-, and $|B_1^-|$-field distributions were compared for the *wo*-IC BC (Figs. 3(a) and (c)) and *w*-IC BC (Figs. 3(b) and (d)). The intensities of the $|B_1|$-fields at the central region were

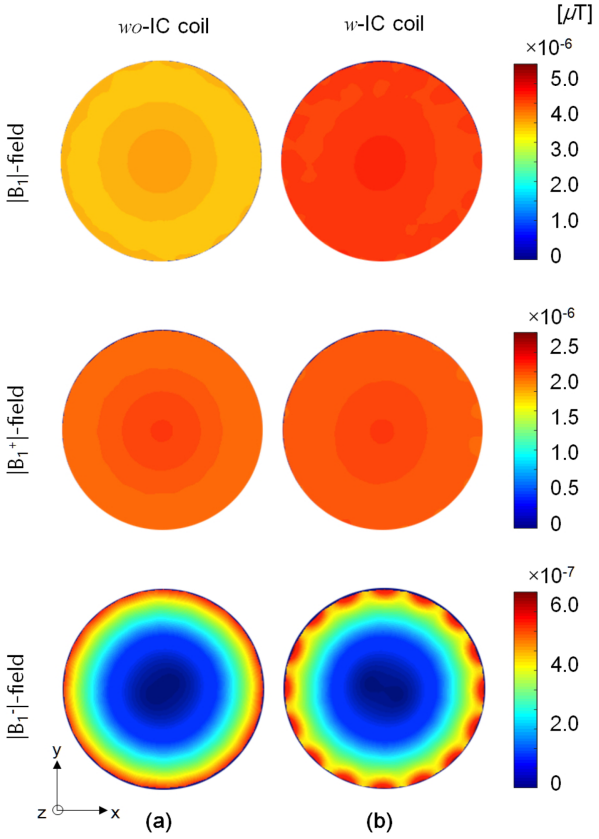

Fig. 2. (Color online) $|B_1|$-, $|B_1^+|$-, and $|B_1^-|$-field distributions using the oil-based phantom: (a) *wo*-IC BC and (b) *w*-IC BC.

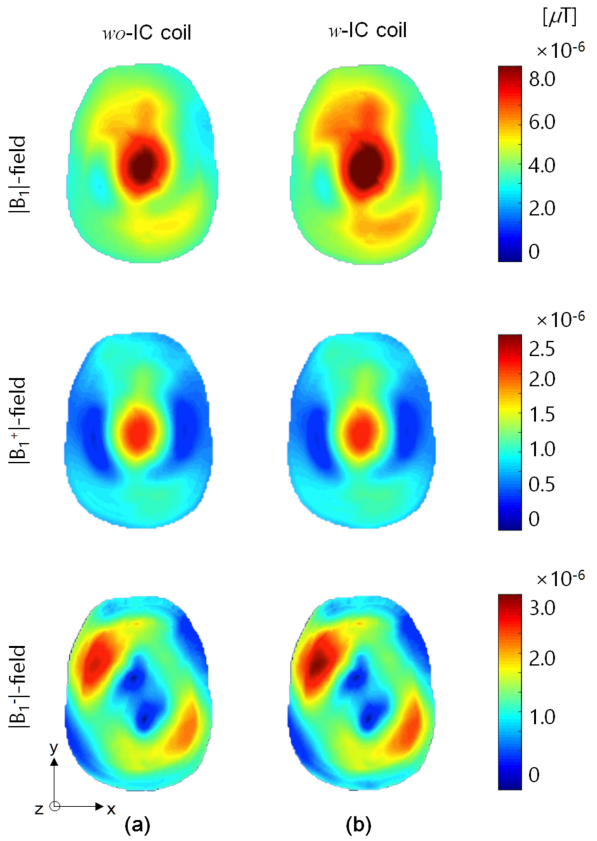

Fig. 3. (Color online) $|B_1|$-, $|B_1^+|$-, and $|B_1^-|$-field distributions using the human-head model: (a) *wo*-IC BC and (b) *w*-IC BC.

measured to be 8.11×10^{-5} and 8.78×10^{-5} μT for the *wo*-IC BC and *w*-IC BC, respectively. The use of the proposed *w*-IC BC shows an 8% enhancement in the $|B_1|$-field sensitivity to that for the *wo*-IC BC. The HF values of the $|B_1^+|$-fields were measured to be 18.40 and 19.70 for the *wo*-IC BC and *w*-IC BC, respectively. The intensities of the $|B_1^-|$-fields at the central region were measured to be 2.71×10^{-6} and 2.91×10^{-6} μT for *wo*-IC BC and *w*-IC BC, respectively.

For the cylindrical phantom and human-head models, although the $|B_1^+|$-fields for the *w*-IC BC and *wo*-IC BC show similar distributions, the $|B_1^-|$-fields do not. These results indicate that the combined geometry of the IC coil array and the BC coil provide an improved sensitivity for the $|B_1^-|$-field instead of the $|B_1^+|$-field. Therefore, the increased sensitivity of the $|B_1^-|$-field indicates an increased $|B_1^-|$-field.

Simulation results for the |E|-field (Figs. 4(a) and (b)) and SAR (Figs. 4(c) and (d)) distributions for the *wo*-IC BC and *w*-IC BC using a human-head model were compared. Similar |E|-field distributions are observed, but with slightly higher |E|-field values for the *w*-IC BC. In addition, the mean SARs were measured to be 0.2087 and 0.2157 W/kg for the *wo*-IC BC and *w*-IC BC, respective-

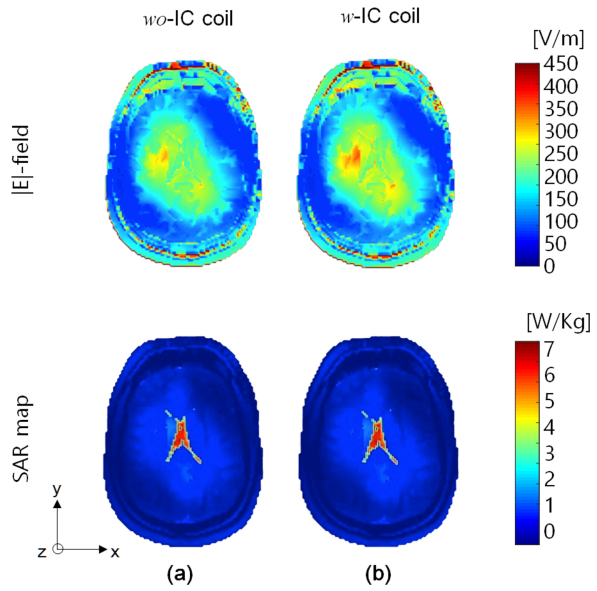

Fig. 4. (Color online) |E|-field and SAR distributions using the human-head model: (a) *wo*-IC BC and (b) *w*-IC BC.

ly, whereas the maximum SAR values were measured to be 8.2034 (*wo*-IC BC) and 8.3755 (*w*-IC BC) W/kg.

4. Conclusion

Herein, we have proposed a new combined geometry of the *w*-IC BC and compared it to the geometry of the *wo*-IC BC. Our calculations show that the *w*-IC BC coil displays enhanced $|B_1|$-field sensitivity. In addition, the SAR value of the *w*-IC BC configuration indicates its suitability and safety for practical use. The proposed *w*-IC BC coil configuration can be effectively adopted in a parallel RF transmission (pTx) system to increase the coil performance in terms of the $|B_1|$-field sensitivity at 7-T and can thus be extended to specific applications in UHF MRI.

Acknowledgment

This research was supported by a grant from the National Research Foundation of Korea (NRF), funded by the Korean Government (MSIP) (no. NRF-2014M3C7033998).

References

[1] D. I. Hoult and P. C. Lauterbur, J. Mag. Reson. **34**, 425 (1979).
[2] V. A. Magnotta, L. Friedman, and F. Birn, J. Digit. Imaging **19**, 140 (2006).
[3] T. S. Ibrahim, R. Lee, B. A. Baertlein, and P. M. L. Robitaille, Phys. Med. Biol. **46**, 609 (2001).
[4] S. Li, Q. X. Yang, and M. B. Smith, Magn. Reson. Imaging **12**, 1079 (1994).
[5] H. Wen, S. C. Andrew, and S. B. Robert, Magn. Reson. Med. **32**, 492 (1994).
[6] F. D. Doty, G. Entzminger, C. D. Hauck, and J. P. Staab, J. Mag. Reson. **138**, 144 (1999).
[7] J. Mispelter, M. Lupu, and A. Briguet, Imperial College, London, **125** (2006).
[8] S. A. Aussenhofer and A. G. Webb, Magn. Reson. Med. **68**, 1325 (2012).
[9] D. I. Hoult, Concepts Magn. Reson. **12**, 173 (2000).
[10] K. N. Kim, J. H. Seo, S. D. Han, H. Song, and Y. Ryu, Electron. Lett. **52**, 591 (2016).
[11] C.M. Collins, Q.X. Yang, J.H. Wang, X. Zhang, H. Liu, S. Michaeli, X.-H. Zhu, G. Adriany, J.T. Vaughan, P. Anderson, H. Merkle, K. Ugurbil, M.B. Smith, and W. Chen, Magn. Reson. Med. **47**, 1026 (2002).